Multiproxy analysis of a new terrestrial and a marine Cretaceous-Paleogene (K-Pg) boundary site from New Zealand

Embaie Ferrow[a,b], Vivi Vajda[a*], Christian Bender Koch[c], Bernhard Peucker-Ehrenbrink[d], Pi Suhr Willumsen[a]

[a] *Department of Earth and Ecosystem Sciences, Lund University, Sölvegatan 12, 223 62 Lund, Sweden*

[b] *Current address: ENAMCO, PO Box 1129, Asmara, Eritrea*

[c] *Department of Basic Sciences and Environment, University of Copenhagen, Thorvaldsensvej 40, DK-1871, Denmark*

[d]*Department of Marine Chemistry & Geochemistry, Woods Hole Oceanographic Institution, Woods Hole, MA 02543-1541, USA*

* Corresponding author:

E-mail address: vivi.vajda@geol.lu.se (V.Vajda)

Abstract

An integrated study of palynology, Mössbauer spectroscopy, mineralogy and osmium isotopes has led to the detection of the first K-Pg boundary clay layer in a Southern Hemisphere terrestrial setting. The K-Pg boundary layer was independently identified at centimetre resolution by all the above mentioned methods at the marine K-Pg boundary site of mid-Waipara and the terrestrial site of Compressor Creek (Greymouth coal field), New Zealand. Mössbauer spectroscopy shows an anomaly of Fe-containing particles in both K-Pg boundary sections: jarosite at mid-Waipara and goethite at Compressor Creek. This anomaly coincides with a turnover in vegetation indicated by an interval dominated by fern spores and extinction of key pollen species in both sections. In addition to the terrestrial floristic changes, the mid-Waipara section reveals a turnover in the dinoflagellate assemblages and the appearance of global earliest Danian index species. Geochemical data reveal relatively small iridium enrichments in the boundary layers of 321 pg/g at mid-Waipara and 176 pg/g at Compressor Creek. Unradiogenic $^{187}Os/^{188}Os$ values of the boundary clay reveal the presence of a significant extraterrestrial component. We interpret the accumulation of Fe nano-phases at the boundary as originating from both the impactor and the crystalline basement target rock. The goethite and jarosite are interpreted as secondary phases formed by weathering and diagenesis. The primary phases were probably controlled by the initial composition of the vapor plume and condensation kinetics rather than condensation thermodynamics. This investigation indicates that identification of Fe in nano-phases by Mössbauer spectroscopy is an accurate and cost-effective method for identifying impact event horizons and it efficiently complements widely used biostratigraphic and geochemical methods.

1. INTRODUCTION

Geochemical, mineralogical, morphological, and paleontological evidence has now shown that the impact of a celestial body in what is now the Yucatán Peninsula in Mexico caused a sudden, dramatic, and global ecological perturbation ~65.5 million years ago (Ma) (Kring, 2007). This event left its imprint as a global clay layer, the so-called Cretaceous-Paleogene (K-Pg) boundary layer (Alvarez et al., 1980; Smit, 1999; Kring, 2007; Schulte et al., 2010). Evidence strongly supporting an impact is provided by the global presence of iridium and other platinum group element (PGE) anomalies (e.g. Alvarez et al., 1980; Kyte, 2002; Claeys et al., 2002; Schulte et al., 2009), the occurrence of high T and high P phases of shocked quartz (Bohor et al., 1984, 1987; Izett, 1990; Claeys et al., 2002), the abundance of tektites and impact related glasses (Izett, 1991; Sigurdsson et al., 1991a, 1991b), and the findings of Ni-rich spinels in the uppermost clay layer that separates the Cretaceous from the Paleogene (Smit and Kyte, 1984; Kyte and Smit, 1986; Robin et al., 1992).

Detailed biostratigraphic studies of New Zealand sediments spanning the K-Pg boundary have been carried out over the last decade (Cooper, 2004, and references therein). The spores and pollen grains produced by land plants are the primary biostratigraphic tools employed to locate the K-Pg boundary in terrestrial settings, whilst transported spores, pollen and in-situ organic-walled dinoflagellate cysts permit identification of the boundary in the shallow marine setting of the mid-Waipara section. The K-Pg boundary in the New Zealand sections is characterized biostratigraphically by a turnover and/or mass extinction of the palynofloras in several terrestrial sections in the coalfields of south-western New Zealand (Vajda et al., 2001, 2003; Vajda and McLoughlin, 2004). A multidisciplinary study based on lithofacies, geochemistry and micropaleontology in marine sediments spanning the K-Pg boundary has revealed that the event is associated with extinctions of calcareous plankton and significant increase in terrigenous clay and biogenic silica (Hollis et al., 1995, 2003a, 2003b).

The presence of nano-particles of oxide and hydroxide in the K-Pg boundary clay at different marine sites has been proposed as additional textural evidence of an extraterrestrial impact (Brooks et al., 1984, 1985; Verma et al., 2001; Wdowiak et al., 2001). However, in sedimentary rocks, magnetically ordered Fe-oxide and hydroxide nano-particles such as hematite, goethite and magnetite, formed by bacterial oxidation and hydrothermal alteration are commonly found associated with clay minerals. Accordingly, such minerals may be identified and characterized by studies of their magnetic properties (Coey, 2009). Our study aims to integrate Mössbauer spectroscopy, mineralogy, osmium isotopes, and biostratigraphy in order to detect impact-generated materials in marine and terrestrial depositional settings. We further aim to determine the origin and mechanism of formation of the texture, composition and morphology of the Fe-bearing nano-particles detected in the Cretaceous-Paleogene boundary layer.

2. GEOLOGICAL SETTING AND SAMPLING

The marine mid-Waipara section is exposed between Doctors Gorge and the Canterbury Plains (172°34’56” E, 43°3’44” S) along the middle reaches of the Waipara River (Fig. 1a), and the K-Pg boundary occurs within a glauconitic sandstone of the upper Conway Formation (Warren and Speden, 1978; Browne and Field, 1985; Hollis and Strong, 2003). The K–Pg boundary is located within the upper Conway Formation, 4 m below its contact to the overlying Loburn Fm. The Conway Formation is a widespread unit typically 100–300 m thick of poorly lithified, medium grey-yellowish, very fine, sandy, siltstone to fine sandstone that commonly exhibits stains on weathered surfaces. In outcrops, the boundary is marked by an irregular ~5 cm thick, Fe-stained zone. Sediments immediately below the Fe-stained zone are calcareous whilst the sediments above this zone are non-calcareous. Bioturbation by marine biota is evident throughout the sequence. Anomalously high concentrations of Ni, Co, and an anomaly of Ir (0.49 ng/g) is associated with this Fe-stained zone (Brooks et al., 1986b). A

new set of samples was collected in 2002 after extensive digging and cleaning of the exposure. A sandstone monolith was cut out with a diamond saw, providing essentially unweathered samples. Twenty-nine samples spanning 0.56 m of the boundary interval were collected and subsequently analysed by Mössbauer spectroscopy, powder X-ray diffraction and palynology. In addition, four samples from the boundary layer were selected for geochemical analyses including $^{187}Os/^{188}Os$ isotope ratios and PGE concentrations. The zero level has been set at the base of the section from mid-Waipara in text and figures.

The Compressor Creek section is exposed in the upper valley of Seven Mile Creek (171°18'35" E, 42°22'31" S) within the Greymouth Coalfield north of Greymouth (Fig. 1a), and is presently located ~150 km from the marine site of mid-Waipara. However, ~65 Ma ago these two sites were located in different basins over 1000 km apart (Fig. 1b). The lithology at Greymouth Coalfield consists of carbonaceous mudstones and siltstones with sporadic coal seams, deposited in a non-marine setting of subsiding floodplains that hosted peat-forming vegetation. Initial biostratigraphic studies spanning a vertical exposure of 7.8 m were carried out, and later high resolution re-sampling targeting the 0.8 metres spanning the K-Pg boundary was performed (Vajda et al., 2003), revealing the exact position of the boundary based on extinction of Maastrichtian key pollen species. For this study, the boundary zone was further sub-sampled with seven splits over a 9 cm interval including the K-Pg boundary (Fig. 2). These samples, herein named CC 1–7, were prepared for Mössbauer spectroscopy, powder X-ray diffraction, and palynology. In addition, four key samples were selected for further geochemical analysis of $^{187}Os/^{188}Os$ isotope ratios and PGE concentrations. The zero level has been set at the base of the studied interval of the Compressor Creek section in text and figures.

3. EXPERIMENTAL METHODS

3.1 X-ray diffraction

Powder X-ray diffraction was used to identify mineral phases to highlight mineralogical heterogeneity between and across the two sections. Diffractograms were obtained using a Siemens D5000 diffractometer equipped with monochromatic Cu- or Co Kα-radiation.

3.2. Mössbauer spectroscopy

The Mössbauer spectra were obtained using a constant acceleration spectrometer and a 25 mCi ^{57}Co source in a Rh matrix. Mössbauer spectra were recorded at two temperatures (30K and 296K for the mid-Waipara and 20K and 296K for the Compressor Creek samples). The low temperature measurements were done using a closed cycle cryostat. Velocities were calibrated using a foil of natural iron at room temperature and isomer shifts are given relative to the centroid of the spectrum of this absorber. Thin absorber tablets were prepared by mixing the sample with a petroleum jelly in a 5 mm thick and 10 mm diameter target to obtain randomly oriented samples (Rancourt, 1994). The spectra were fitted using the Lorentzian site analysis software program in Recoil, a commercially available Mössbauer spectral analysis software package. Each absorber was made from 50 mg of sample. Experimental points are shown as dots and fit components and sum of fit components are shown as continuous lines.

3.3. Palynological processing

Palynological processing followed standard methods: 10-20 g of sample was treated with hydrochloric acid (HCl) to remove carbonate before the rock matrix was digested with hydrofluoric acid (HF) to remove siliciclastic material (Batten, 1999). The organic matter

residue was sieved and retained on a 6 μm screen. The organic residue was mounted on slides in glycerine jelly and sealed for examination under a transmitted light microscope. Percentages of spores, pollen, and dinoflagellates were calculated from a total counted population of at least 300 specimens per sample. The slides were further examined to check for the presence of rare taxa. Slides and macerated residues of the samples are deposited at the Institute of Geological & Nuclear Sciences, Lower Hutt, New Zealand.

3.4. Osmium isotopes

Platinum group elements and $^{187}Os/^{188}Os$ isotope ratios were determined using standard procedures used at the Woods Hole Oceanographic Institution. A few grams of sample powder were mixed with an isotopically enriched tracer solution of ^{99}Ru, ^{105}Pd, ^{190}Os, ^{191}Ir, and ^{198}Pt, and the tracer solution was dried over night at room temperature. Then, borax, Ni and S powder were added to the sample-tracer mix, homogenized, and fused in a glazed ceramic crucible for 90 minutes at 1050°C in a muffle furnace following procedures described by Ravizza and Pyle (1997). Osmium isotopes were determined by multicollector ICPMS (ThermoFinnigan Neptune) using a multidynamic data acquisition routine with three continuous dynode electron multipliers. Osmium was introduced as OsO_4 following methods described by Hassler et al. (2000). We determined PGE concentrations in the liquid residue after Os isotope analyses using a single-collector ICPMS (ThermoFinnigan Element2). Accuracy and precision of these analytical methods have been described in detail by Peucker-Ehrenbrink et al. (2003).

4. EXPERIMENTAL RESULTS AND INTERPRETATION

4.1 XRD

The XRD patterns for mid-Waipara and Compressor Creek (see Fig. 3) show that the major mineral components in the samples from mid-Waipara are quartz, feldspar, smectite/illite, and kaolinite. The dominant minerals present at Compressor Creek are quartz, illite, kaolinite and chlorite. In addition, mid-Waipara sample MW-13 (within the K-Pg boundary layer) shows diffraction peaks compatible with those of jarosite, and traces of gypsum are indicated in other samples from Compressor Creek. Samples CC-3 and CC-4 (within the K-Pg boundary layer) show weak peaks due to the presence of minor goethite and pyrite.

4.2 Mössbauer spectroscopy

Representative Mössbauer spectra of three samples from mid-Waipara (one sample below the boundary MW-10, one within the boundary layer MW-13, and one above the boundary MW-15) taken at 296K and 30K and fitted using Lorentzian line shapes are shown in Fig. 4. Since glauconite is the dominant silicate phase identified by optical microscopy and X-ray diffraction that contains Fe in its structure, the observed Mössbauer spectra are attributed to this mineral.

Published Mössbauer spectra of glauconite show that the absorption lines for both octahedrally coordinated ferrous and ferric iron, $^{[6]}Fe^{3+}$ and $^{[6]}Fe^{2+}$, are broad and overlapping (Rongchuan et al., 1986; Cardile and Brown, 1988; Ali et al., 2001, Kuzmann et al., 2003). These observations indicate that Fe in glauconite is distributed between the two types of octahedrally coordinated cation sites, designated M1 and M2, in the crystals. At 296K, the Mössbauer spectra of samples MW-15 and MW-10 were fitted using three doublets, two for distinct $^{[6]}Fe^{2+}$ sites at M1 and M2 and one for overlapping $^{[6]}Fe^{3+}$ sites at M1 and M2. At 30K, however, only two doublets were used, each for overlapping $^{[6]}Fe^{2+}$ and $^{[6]}Fe^{3+}$ at M1

196 and M2 sites. These observations are valid for all the other samples taken above and below
197 the K-Pg boundary.

198 The Mössbauer spectra of sample MW-13 show additional features compared to the
199 spectra of samples above and below the K-Pg boundary. The 296K spectrum of sample MW-
200 13 (Fig. 4), for example, shows the presence of a distinct shoulder (vertical arrows) due to the
201 presence of an additional Fe-bearing phase with isomer shift and quadrupole splitting of 0.39
202 mm/s and 1.20 mm/s, respectively. These parameters correspond to the Mössbauer parameters
203 of jarosite as reported in the literature (Leclerc, 1980; Bigham and Nordstrom, 2000).
204 Moreover, the disappearance of the doublet at 296K and its replacement by a sextet at 30K
205 (vertical arrows) with a magnetic hyperfine field of 44 Tesla confirms that the additional Fe-
206 bearing phase found at the K-Pg in mid-Waipara is indeed jarosite, because jarosite shows
207 magnetic ordering at 30K (Eneroth and Bender Koch, 2004) similar to those jarosite-bearing
208 gypsum-rich sediments reported from Moscow Landing and Starkville (Wdowiak et al.,
209 2001). The detection of jarosite at the K-Pg in mid-Waipara by Mössbauer spectroscopy
210 corroborates the observation made by X-ray diffraction.

211 It has been established that, for a given number of free parameters, fitting the Mössbauer
212 spectra of phyllosilicates with overlapping Mössbauer lines assuming a distribution of
213 quadrupole splitting (QSD) produces a better approximation of the relative distribution of Fe
214 species in the different sites than does fitting the spectra assuming a Lorentzian line shape for
215 the absorption lines (Rancourt, 1994; Ferrow, 2002; Kuzmann et al., 2003). Consequently, in
216 this study the spectra of the glauconite-containing samples were also fitted assuming that the
217 electrical quadrupole splitting was distributed, and Mössbauer data of Longworth et al. (1986)
218 and Ferrow (1987) were used to assign the Fe species to the M1 and M2 sites (Table 1).
219 According to Ali et al. (2001), the Mössbauer parameters of glauconite are very sensitive to
220 the environmental conditions prevailing during glauconitization. For example, with increasing

degree of glauconitization the ratios of $^{[6]}Fe^{3+}/^{[6]}Fe^{2+}$ and $^{[6]}Fe^{3+}$(M2)/$^{[6]}Fe^{3+}$(M1) increase, i.e. the maturation process is accompanied by oxidation of $^{[6]}Fe^{2+}$ to $^{[6]}Fe^{3+}$and a corresponding increase of $^{[6]}Fe^{3+}$ in the M2 site. Data in Fig. 5a show remarkably constant $^{[6]}Fe^{3+}/^{[6]}Fe^{2+}$ ratios throughout the section, indicating that the depositional environment was relatively stable over periods defined by the sample resolution. However, the presence of relatively high $^{[6]}Fe^{2+}$ abundances (20%) in glauconite from mid-Waipara indicates that the maturation process was incomplete in these sediments. The distribution of $^{[6]}Fe^{3+}$ between M1 and M2 sites (Fig. 5b) shows two distinct erratic intervals between samples MW-11 and MW-21 with maximum anomaly in sample MW-13 and quite stable regions above and below this interval. The increase in $^{[6]}Fe^{3+}$at the M2 site in these two samples is explained as an artefact caused by inclusion of the jarosite spectral component into the fit of glauconite.

Representative Mössbauer spectra of the samples from Compressor Creek, taken at 296K and 20K and fitted using components with Lorentzian line shapes, are shown in Fig. 6. The Mössbauer spectrum of the boundary clay layer (sample CC-3) shows line broadening and a poorly defined magnetically-ordered sextet at 296K due to the presence of nano-sized goethite (Madsen et al., 2009).

Based on the Mössbauer parameters derived from the 20K analyses and from the X-ray data in Fig. 3 we assign the $^{[6]}Fe^{2+}$ to chlorite, the paramagnetic $^{[6]}Fe^{3+}$ to illite - with minor contribution of chlorite (Wagner et al., 1990) - and the magnetically ordered sextet to goethite (Mørup et al., 1983). Moreover, the highest amount of Fe in goethite at Compressor Creek is associated with the boundary clay layer (sample CC-3), whereas samples above the boundary (samples CC-5 and CC-7) contain Fe in paramagnetic minerals only (Figs. 6, 7). The relatively large amount of nano-particles of goethite observed below the K-Pg boundary (samples CC-2 and CC-1) suggests post-depositional downward transport of these nano-sized particles within the sediments. Such transport has previously been observed for shocked

246 quartz as well as iridium and other elements at other terrestrial and marine K-Pg sites
247 (Peucker-Ehrenbrink et al., 1995; Zhou et al., 2001; Vajda and McLoughlin, 2004, 2007). The
248 nano-particles are smaller than 15 nm, which increases the probability of these particles to be
249 dispersed downward within the sediments.

250 Variations in the Fe-species in Compressor Creek samples (Table 2), derived from low-
251 temperature Mössbauer analyses, show an increase in the amount of nano-phase goethite at
252 the K-Pg (Fig. 7a). For the mid-Waipara section the anomaly is very sharp despite the small
253 amount of the jarosite and is found exclusively at the K-Pg boundary. Data for Compressor
254 Creek, in contrast, indicate that goethite also occurs in samples below the boundary.

255

256 **4.3 Osmium isotopes**

257 Iridium concentrations in the K-Pg boundary layer at the two sites are significantly higher
258 than upper crustal levels of approximately ~22 pg/g (Peucker-Ehrenbrink and Jahn, 2001;
259 Peucker-Ehrenbrink et al., 2003). However, concentrations are low compared to the nearby
260 terrestrial K-Pg site of Moody Creek Mine, where an anomaly of 4ng/g has been reported
261 (Vajda and McLoughlin, 2004). Iridium concentrations are comparable to those at the marine
262 Woodside Creek site (0.49 ng/g; Brooks et al., 1984, 1986). In the terrestrial location
263 (Compressor Creek) Os and Ir concentrations are similar, particularly in sample CC-3 that
264 marks the K-Pg. In this sample the Os/Ir ratio is chondritic. In contrast, the marine location
265 (mid-Waipara) has more fractionated Os/Ir values with significantly higher Os concentrations.
266 This is typically observed in marine sediments with elevated organic carbon contents, because
267 Os is more efficiently scavenged than Ir by such sediments.

268 Osmium isotope ratios ($^{187}Os/^{188}Os$) are significantly less radiogenic than average eroding
269 continental crust ($^{187}Os/^{188}Os \sim 1.05$, Peucker-Ehrenbrink and Jahn, 2001) and are much more

similar to extraterrestrial ($^{187}Os/^{188}Os$ ~0.12-0.14) and mantle-derived Os. Osmium isotope values at the time of deposition were likely even less radiogenic than the measured values, because the values we report have not been corrected for radiogenic ingrowth since deposition. This would have required the determination of Re concentrations. The measured $^{187}Os/^{188}Os$ values at the K-Pg boundaries in both sites are, within uncertainty, the least radiogenic values of the entire sample set.

The PGE and $^{187}Os/^{188}Os$ data (Table 3) are consistent with significant contributions from an extraterrestrial (chondritic) impactor to the sedimentary PGE budget.

4.4. Palynology

The shallow marine sediments at mid-Waipara contain a transported but well-preserved assemblage of spores and pollen grains, and 50 species of fossil pollen and spores from terrestrial land plants were identified in this study. Based on changes in relative abundance of different pollen-spore groups as well as the last appearance of *Tricolpites lilliei* and first appearance datum (FAD) of key taxa, the K-Pg boundary is located in sample MW-13, 24 cm above the base of the sampled section (Fig. 8a), that is also recognized by the fern-spike, starting in sample MW-13. The fern spike extends for 18 cm above the boundary (including sample MW-22). The base of the fern-spike clearly indicates the onset of altered ecological conditions that presumably have been caused by the Chicxulub impact (Nichols and Johnson, 2002; Vajda and Raine, 2003; Pole and Vajda, 2009).

A diverse assemblage of marine organic-walled dinoflagellates cysts comprising 93 species was recorded in the samples from mid-Waipara. The K-Pg boundary interval in mid-Waipara (between sample MW-12 and MW-13; Fig. 8a) coincides with the FAD of a number of global earliest Danian taxa such as *Damassadinium californicum*, *Senoniasphaera inornata*

294 and *Membranilarnacia tenella* (Moshkovitz and Habib, 1993; Habib et al., 1996; Stover et al.,
295 1996; Williams et al., 2004). The FAD of these Danian index taxa dinoflagellate cysts further
296 supports application of Mössbauer signals in locating potential K-Pg horizons. Two sporadic
297 occurrences of *C. cornuta* below the K-Pg boundary in samples MW12 and MW10 are
298 considered artefacts of reworking by intense bioturbation of the sediments at the K-Pg
299 transition (see discussion in Willumsen, 2006, p. 959). However, the dinoflagellate species
300 *Trithyrodinium evittii* has its FAD in sample MW-13 and it becomes increasingly abundant up
301 through the basal 20 cm of Danian strata examined, which supports previous observations
302 from this section as well as patterns reported elsewhere in New Zealand K-Pg boundary
303 sections (Wilson, 1987; Willumsen, 2000, 2003, 2004, 2006; Willumsen, in press).

304 The interval 2-23 cm (samples MW-1 to MW-12) belongs to the *Manumiella druggii*
305 Interval Zone, whereas the interval from 24 cm (sample MW-13 to MW-27) is placed within
306 the *T. evittii* Interval Zone (Helby et al., 1987; Wilson, 1984, 1987; Willumsen, in press)
307 (Figs. 5 and 8a). Noteworthy, both *Manumiella druggii* and *M. seelandica* co-occur with the
308 earliest Danian marker species directly above the boundary where they are also relatively
309 more common than in the latest Maastrichtian sediments (Willlumsen, 2000, 2003, 2006).
310 *Carpatella septata* occur from the base of the latest Maastrichtian strata upwards and it
311 disappear in the earliest Danian, supporting previous observations by Willumsen (2000, 2003,
312 2004, 2006, in press). *Palynodinium minus* has its FAD in sample MS-6 (12cm below the K-
313 Pg boundary) and occurs consistently throughout the Danian strata examined.

314 Variations in microfossils from both the terrestrial plant and marine plankton assemblages
315 from the mid-Waipara River section suggest that the change from the latest Maastrichtian to
316 Danian flora is not as abrupt as the floral change at the Compressor Creek section. At mid-
317 Waipara River, Cretaceous terrestrial indicator species such as *Nothofagidites kaitangata* and
318 *Tricolpites lilliei* are identified above the K-Pg boundary, a clear sign of bioturbation and

reworking. This interpretation is further supported by the higher diversity seen in the palynological assemblage at mid-Waipara compared to Compressor Creek. We interpret this observation as a result of the larger catchment area of the sediments at this near-shore marine site. Thus, at mid-Waipara the agreement between the Mössbauer signal and the palynological signal is striking, as Fe in paramagnetic state occurs throughout the fern-spike interval.

The samples from Compressor Creek contain a well-preserved miospore assemblage, and 34 species of pollen and spores were identified. No marine palynomorphs were encountered in this entirely terrestrial setting. Based on the last appearance datum (LAD) of indicator species such as *Tricolpites lilliei* and *Nothofagidites kaitangata*, the two pollen zones *Phyllocladidites mawsonii,* PM2 and PM3 as outlined by Raine (1984) (see further Vajda and Raine, 2010), were identified (Fig. 8b). The K-Pg boundary was located at sample CC-3 at the base of the 1 cm thick clay layer which also marks the base of the PM3 pollen zone. The boundary is also marked by a sharp and sudden increase in fern spores. This marked increase, from 34% below the boundary to 74% above it, is mainly caused by the increase in the spores *Baculatisporites comaumensis* and *Cyathidites* spp., representing ground fern and tree ferns, respectively. The high relative abundance of fern spores persists in the overlying five centimetres that define the basal part of the so-called fern-spike (Fig. 8b). This is consistent with the results from another adjacent terrestrial K-Pg section, Moody Creek Mine, where the boundary is located within a coal seam (Vajda et al., 2001; Vajda and McLoughlin, 2004).

5. FORMATION MECHANISM AND SOURCE OF K-Pg NANO-PARTICLES

The mineralogy of the nano-phases at the investigated K-Pg boundary sites is dominated by goethite, although phases such as jarosite, hematite, and magnetite have also been reported

343 (Brooks et al., 1985; Griscom et al., 1999; Wdowiak et al., 2001; Verma et al., 2001;
344 Bhandari et al., 2002). We argue that the variation in the mineralogy of nano-particles
345 observed at the two K-Pg boundary sites merely reflects the prevailing post-depositional
346 diagenetic conditions rather than the primary mineralogy of the nano-particle condensed after
347 the impact.

348 The target rock at Chicxulub is composed of a 3 km thick succession of limestones,
349 anhydrite, dolomite, marls and sandstones covering crystalline basement (Kettrup and
350 Deutsch, 2003). When the impactor hit the target rock, the carbonate platform and the
351 underlying crystalline basement were excavated, involving material down to the base of the
352 crust (Kring, 2005). Stephens and Kothari (1978) indicated that the condensate collected from
353 experiments in reactive gas atmospheres reflects both the composition of the target and the
354 ambient gas. Consequently, a sulfide aerosol formed from the vaporization of anhydrite and
355 associated massive addition of CO_2 by impact vaporization of the carbonate platform at
356 Chicxulub (O'Keefe and Ahrens, 1989; Pope et al., 1994; Ocampo et al., 2006; Wigforss-
357 Lange et al., 2007) provided an environment conducive to the condensation of Fe-sulfide
358 phases. Well crystallized phases, however, are unlikely to occur owing to the non-equilibrium
359 nature of condensation that favors the formation of metastable rather than thermodynamically
360 stable phases (Hirth and Pound, 1963; Dunning, 1969; Donn, 1979). We contend that the Fe
361 in the Fe-sulfides is derived from the impactor. One aspect of the vapor ejecta that is often
362 overlooked is its reaction with the atmosphere. Although there will be a condensation phase
363 as the vapor plume rises from the crater and into space, it will be re-heated when it re-enters
364 the atmosphere. Therefore, there may be a second episode of (partial) evaporation and
365 condensation. This process did not vaporize all of the solid debris in the plume, as indicated
366 by the shocked quartz that excavated from the target survives and was deposited around the
367 world. The presence of shocked quartz also illustrates the heterogeneous nature of the

process. Although the vapor plume contained a lot of vaporized rock components, it also contrained solid quartz, feldspar, and other crystalline phases.

We agree with the assessment of Brooks et al. (1985) that the nano-particles identified in the K-Pg clays at several sites are post-depositional authigenic products. We also agree that jarosite could be formed by bacterial oxidation of pyrite (Carlson et al., 1992). However, we argue that marcasite and not pyrite is the most probable primary condensate, as the former is metastable at temperatures below 700K and subsequently converts to pyrite (Lennie and Vaughan, 1992).

Although the mineralogy of the nano-particles associated with the K-Pg layer reflects post-depositional diagenetic alteration, the impact-induced texture and morphology remain primary. Stephens and Kothari (1978) developed a conceptual model of the vaporization, condensation, and grain-gas interaction that accounts well for the formation of nano-particles, their morphology and their mineralogy at K-Pg boundary sites. These authors argued that preservation of small grain sizes was facilitated by rapid expansion of the target vapor and rapid mixing with cold ambient gas. This causes the vapor to become supersaturated within microseconds and to nucleate into ~1 nm droplets. Further growth occurs predominantly by droplet collisions due to thermal motions, and to some extent by aerosol growth via thermal coagulation. Stephens and Kothari (1978) showed that the resulting condensate smoke consists, in most cases, of strings composed of grains that have a median diameter of 20–30 nm. Moreover, as droplet size decreases, surface energy becomes comparable in magnitude to the binding energy of the atoms in the droplet volume, tending to promote the formation of spherical grains (Stephens and Kothari, 1978). We suggest that the growth mechanisms of nano-sized and spherical particles described in the experimental work of Stephens and Kothari (1978) explains well the formation mechanism of nano-particles with spheroidal morphology such as those identified in the K-Pg boundary clay.

393 Nano-particles of Fe-oxides, Fe-sulphates, and Fe-hydroxides such as hematite, magnetite,
394 jarosite and goethite, formed by hydrothermal alteration and bacterial oxidation, are
395 commonly found in sedimentary rocks. Jarosite, for example, develops naturally through the
396 weathering of pyrite, and it can also be formed during bioleaching of iron-containing sulfides,
397 especially by thermophile bacteria (Larsson et al., 1990). Moreover, jarosite has also been
398 found in various plants as a product of biomineralization processes (Rohwerder et al., 2003),
399 Allen et al. (1999) suggested a link between as yet unidentified marine biogenic gas emissions
400 and nano-particle formation and it has also been suggested that nano-particles identified at the
401 K–Pg boundary were formed by similar diagenetic and biogenic processes (Villasante et al.,
402 2009). However, it is difficult to explain why such processes, especially hydrothermal
403 alteration, should be confined to a thin, well-defined globally distributed clay bed at the K–Pg
404 boundary. If the nano-particles found associated with K–Pg boundary were formed by
405 biological processes, then the widespread but stratigraphically narrow occurrence of the nano-
406 particles in well-dated sections would indicate a surge in biologic activity and massive
407 production of biogenic gas in the immediate aftermath of the Chicxulub impact.
408 A detailed rock magnetic study of K-Pg boundary sediments from an ODP section from
409 the southern Kerguelen Plateau by Abrajevitch and Kodama (2009) reveals that cessation of
410 biological productivity after the event allowed preservation of the initial detrital authigenic
411 iron phases (dominated by reactive iron oxyhydroxides). The oxyhydroxides, however, were
412 replaced with biogenic magnetite as the recovery of normal biological activity took place,
413 leading to the production of biochemical magnetization and to a several-fold increase in
414 remanence (Abrajevitch and Kodama 2009). Their results suggest that in areas where
415 bioavailable iron constitutes a significant part of the detrital input, such as in pelagic marine
416 environments distant from clastic sources, the biochemical remanent magnetization may be
417 the dominant process of magnetization acquisition (Abrajevitch and Kodama 2009).

418 The origin of the nano-particles by atmospheric condensation and global fallout appears to
419 be a more parsimonious explanation for their distribution.
420

421 **6. CONCLUSIONS**

422 This integrated study has led to the detection of the first K-Pg boundary clay layer in a
423 Southern Hemisphere terrestrial setting. All methods employed place the boundary, at
424 centimetre resolution, in the same horizon both in the marine sequence of mid-Waipara and in
425 the terrestrial K-Pg boundary site at Compressor Creek. At mid-Waipara Mössbauer
426 spectroscopy, osmium isotopes and biostratigraphy identify sample MW-13 at 24 cm above
427 the base of the investigated section as the K-Pg boundary layer (Figs. 5, 8a). Osmium isotope
428 values indicate a significant extraterrestrial component within the same sample. Similarly, the
429 boundary clay at Compressor Creek is located at the base of sample CC-3, making it the first
430 continental boundary clay identified in the Southern Hemisphere (Figs. 7, 8b).
431 Nano-particles are commonly found associated with the K-Pg boundary. Their texture and
432 morphology is primary as modeled by Stephens and Kothari (1978), and not characteristic of
433 hydrothermal or biologic processes. The experimental model suggests that the ~ 1 nm droplets
434 as the target rock and impactor are vaporized, ejected at supersonic speed into the stratosphere
435 and cooled extremely rapidly. Grain growth is influenced by the density of the original
436 condensate droplets, circulation within the ejecta plume, and aerosol growth via thermal
437 coagulation. Furthermore, the experimental data showed that the resulting condensate smoke
438 consists, in most cases, of strings made up of grains with a median diametre of 20–30 nm, in
439 full agreement with our observations.
440 The Fe-bearing nano-phases in the K-Pg boundary clays consist of goethite, jarosite,
441 hematite, magnetite and pyrite — phases commonly found associated with clay minerals in
442 sedimentary rocks. However, the composition of these Fe-phases in the boundary clay is not

primary but a result of diagenetic alteration since deposition ~ 65 Ma. It is most likely that the primary impact-related Fe-phases were metastable Fe-sulphides, as determined by the chemistry of the target and impactor (Kring, 2005). Moreover, the condensation environment with temperatures below 700K favours the formation and 'freezing in' of metastable products rather than the occurrence of the thermodynamically stable species (Donn, 1979). We suggest that the Fe-sulphide condensate was probably marcasite, and not pyrite as proposed by Brooks et al. (1985).

Finally, this investigation clearly demonstrates that Mössbauer spectroscopy is a simple, fast, sensitive, and accessible technique for detecting Fe-bearing phases associated with impact events. Another advantage is that Mössbauer measurements do not alter the samples, which allows them to be subsequently investigated with other techniques.

ACKNOWLEDGMENTS

We thank the reviewers David Kring (LPI) and Peter Schulte (Erlangen University) and associate editor Uwe Reimold for their constructive criticism and comments that significantly improved this paper. We thank Rob Boyd and Solid Minerals for giving us access to their property, Ian Raine for assistance in the field, and John Simes and Christopher Hollis for providing samples from mid-Waipara. Tracy Atwood and Jerzy Blusztajn helped with the PGE and Os isotope analyses that were carried out in the NSF-supported WHOI ICPMS Facility. E. Ferrow acknowledges the support rendered by Berhane Habtemariam, the general manager of Enamco, during the final review of the paper. V. Vajda acknowledges the financial support provided by the Swedish Royal Academy of Sciences through the Knut & Alice Wallenbergs Foundation and from the Crafoord Foundation. P.S. Willumsen acknowledges financial support from the Carlsberg Foundation no.2008_01_0404.

REFERENCES

Abrajevitch A. and Kodama K. (2009) Biochemical vs. detrital mechanism of remanence acquisition in marine carbonates: A lesson from the K-T boundary interval. *Earth Planet. Sci. Lett.* **286**, 269–277.

Allen A. G., Grenfell J. L., Harrison R. M., James J. and Evans M. J. (1999) Nanoparticle formation in marine airmasses: contrasting behaviour of the Open Ocean and coastal environments. *Atmos. Res*. **51**, 1–14.

Ali A. M., Hsia Y., Liu R., Zhang J., Duan W. and Chen L. (2001) A Mössbauer study of evolution of glauconite from Chinese seas. *Spectrosc. Lett.* **34**, 701–708.

Alvarez L.W., Alvarez W., Asaro F. and Michel, H. V. (1980) Extraterrestrial cause for the Cretaceous–Tertiary extinction. *Science* **208**, 1095–1108.

Batten D. J. (1999) Small palynomorphs. In *Fossil Plants and Spores: modern Techniques* (eds. T. P. Jones and N. P. Rowe). *Geological Society of London*, London, 15–19.

Bhandari N., Verma H. C., Upashyay C., Tripathy A. and Tripathy R.. P. (2002) Global occurrence of magnetic and superparamagnetic iron phases in Cretaceous–Tertiary boundary clays. In *Catastrophic events and mass extinctions: impacts and beyond* (eds. C. Koeberl and K. G. MacLeod). Boulder, Colorado. *Geol. Soc. Spec. Paper*, vol 356, pp. 201–211.

Bigham J. M. and Nordstrom D. K. (2000) Iron and aluminum hydroxysulfates from acid sulfate waters. In *Sulfate Minerals* (eds. C. N. Alpers, J. L. Jambor and D. K. Nordstrom). *Reviews in Mineralogy and Geochemistry* 40, *Mineral. Soc. Am.*, pp. 351–403.

492 Bohor B. F., Foord E. E., Modreski P. J. and Triplehorn D. M. (1984) Mineralogic
493 evidence for an impact event in the Cretaceous–Tertiary event. *Science* **224**, 867–
494 869.

495 Bohor B. F., Modreski P. J. and Foord E. E. (1987) Shocked quartz in the Cretaceous–
496 Tertiary boundary clays – evidence for a global disruption. *Science* **236**, 705–709.

497 Brooks R. R., Reeves R. D., Xing–Hua Y., Ryan D. E., Holzbecker J., Collen J. D., Neall V.
498 E. and Lee J. (1984) Elemental anomalies at the Cretaceous–Tertiary boundary,
499 Woodside Creek, New Zealand. *Science* **226**, 539–542.

500 Brooks R. R., Hoek P. L., Reeves R. D., Wallace R. C., Johnston J. H., Ryan D. E.,
501 Holzbecher J. and Collen J. D. (1985) Weathered spheroids in a Cretaceous/Tertiary
502 boundary shale at Woodside Creek, New Zealand. *Geology* **13**, 738–740.

503 Brooks R. R., Strong C. P., Lee J., Orth C. J., Gilmore J. S., Ryan D. E. and Holzbecher J.
504 (1986) Stratigraphic occurrences of iridium anomalies at four Cretaceous/Tertiary
505 boundary sites in New Zealand. *Geology* **14**, 727–729.

506 Browne G. H. and Field B. D. (1985) The lithostratigraphy of Late Cretaceous to Early
507 Pleistocene rocks of northern Canterbury, New Zealand. *New Zead. Geol. Surv. Rec.*
508 **6**, 63 pp.

509 Cardile C. M. and Brown I. W. M. (1988) An 57Fe Mössbauer spectroscopic and X–ray
510 diffraction study of New Zealand glauconite. *Clay Miner*. **23**, 13–25.

511 Carlson L., Lindstrom E. B., Hallberg K. B. and Tuovinen O. H. (1992) Solid–Phase
512 Products of Bacterial Oxidation of Arsenical Pyrite. *Appl. Environ. Microb*. **58**,
513 1046–1049.

514 Claeys P. H., Kiessling W. and Alvarez W. (2002) Distribution of Chicxulub ejecta at the
515 Cretaceous–Tertiary boundary. In *Catastrophic events and mass extinction: impacts*

516 *and beyond* (eds. C. Koeberl and K. G. MacLeod) Boulder, Colorado. *Geol. Soc.*
517 *Spec. Paper*, vol. 356, 55–68.

518 Coey, J. M. D. (2009) Magnetism and Magnetic Materials, Cambridge University Press,
519 pp. 604

520 Cooper R. A. (2004) The New Zealand Geological Timescale. *Institute of Geological &*
521 *Nuclear Sciences Monograph* **22**, 284pp.

522 Donn B. (1979) Some aspects of condensation in clouds. *Astrophys Space Sci* **65**, 167–171.

523 Dunning W. J. (1969) General and theoretical introduction in nucleation. In *Nucleation*
524 *Phenomena* (ed. A. C. Zettlemoyer), 167pp.

525 Eneroth E. and Bender Koch C. (2004) Fe–hydroxysulphates from bacterial Fe^{2+}oxidation.
526 *Hyperfine Interactions* **156/157**, 423–429.

527 Ferrow E. (1987) Mössbauer effect and X–ray diffraction studies of synthetic iron bearing
528 tetrahedral micas. *Phys. Chem. Minerals*. **14**, 276–280.

529 Ferrow E. (2002) Experimental weathering of biotite, muscovite and vermiculite: a
530 Mössbauer spectroscopy study. *Eur. J. Mineral*. **14**, 85–95.

531 Griscom D. L., Beltran–Lopez V., Merzbacher C. I. and Bolden E. (1999) Electron spin
532 resonance of 65–million–year–old glasses and rocks from Cretaceous–Tertiary
533 boundary. *J. Non–Cryst. Solids* **253**, 1–22.

534 Habib D., Olsson R.K. and Lui C. (1996) High–resolution biostratigraphy of sea–level low,
535 biotic extinction, and chaotic sedimentation at the Cretaceous–Tertiary boundary in
536 Alabama, north of the Chicxulub crater. In: *The Cretaceous–Tertiary event and other*
537 *catastrophes in Earth history* (eds. G. Ryder and S. Gartner). Boulder, Colorado. *Geol.*
538 *Soc. Spec. Paper*, vol. **307**, 243–252.

539 Hassler D. R., Peucker–Ehrenbrink B. and Ravizza G. E. (2000) Rapid determination of Os
540 isotopic compositions by sparging OsO_4 into a magnetic–sector ICP–MS. *Chem. Geol*.,
541 **166**, 1–14.

542 Helby R., Morgan R. and Partridge, A. D. (1987) A palynological zonation of the Australian
543 Mesozoic. In: *Studies in Australian Mesozoic Mesozoic Palynology* (ed. P. A. Jell)
544 *Assoc. Australas. Paleontol. Mem*. vol 4, pp. 1–94.

545 Hirth J. P. and Pound C. M. (1963) Condensation and Evaporation, 1-41. McMillan, New
546 York.

547 Hollis C. J., Rodgers K. A. and Parker R. J. (1995). Siliceous plankton bloom in the earliest
548 Tertiary of Marlborough, New Zealand. *Geology* **23**, 835–838.

549 Hollis C. J. and Strong, C. P. (2003) Biostratigraphic review of the Cretaceous/Tertiary
550 boundary transition, mid–Waipara River, North Canterbury, New Zealand. *New Zeal.*
551 *J. Geol. Geop*. **46**, 243–254.

552 Hollis C. J., Strong C. P., Rodgers K. A. and Rogers K. M. (2003a) Paleoenvironmental
553 changes across the Cretaceous/Tertiary boundary at Flaxbourne River and Woodside
554 Creek, eastern Marlborough, New Zealand. *New Zeal. J. Geol. Geop*. **46**, 177–198.

555 Hollis C. J., Rodgers K. A., Strong C. P., Field B. D. and Rogers, K. M. (2003b)
556 Palaeoenvironmental changes across the Cretaceous/Tertiary boundary at the
557 northern Clarence Valley, southeastern Marlborough, New Zealand. *New Zeal. J.*
558 *Geol. Geop*. **46**, 209–234.

559 Izett G. A. (1990) The Cretaceous/Tertiary Boundary Interval, Raton Basin Colorado and
560 New Mexico. Boulder, Colorado. *Geol. Soc. Spec. Paper,* vol. *249*, 1–100.

561 Izett G. A. (1991) Tektites in Cretaceous–Tertiary boundary rocks on Haiti and their
562 bearing on the Alvarez Impact extinction hypothesis. *J. Geophys. Res*. **96**, 20879–
563 20905.

564 Kettrup B. and Deutsch A. (2003) Geochemical variability of the Yucatan basement:
565 constraints from crystalline clasts in Chicxulub impactites. *Meteorit. Planet. Sci.* **38**,
566 1079–1092.

567 Kring D. A. (2007) The Chicxulub impact event and its environmental consequences at the
568 Cretaceous-Tertiary boundary *Palaeogeogr. Palaeoclimatol. Palaeoecol.* **255**, 4–21.

569 Kring D. A. (2005) Hypervelocity collisions into continental crust composed of sediments
570 and an underlying crystalline basement: comparing the Ries and Chicxulub impact
571 craters. *Chem. Erde–Geochem*. **65**, 1–46.

572 Kuzmann E., Nagy S. and Vertes A. (2003) Critical review of analytical applications of
573 Mössbauer spectroscopy illustrated by mineralogical and geological examples. *Pure*
574 *App. Chem.* **75**, 801–858.

575 Kyte F. T. (2002) Tracers of the extraterrestrial components in sediments and inferences
576 for Earths´ accretion history. In *Catastrophic events and mass extinction: impacts*
577 *and beyond* (eds. C. Koeberl and K.G. MacLeod) Boulder, Colorado. *Geol. Soc.*
578 *Spec. Paper,* vol. 356, 21–38.

579 Kyte F. T. and Smit J. (1986) Regional variations in spinel compositions: an important key
580 to the Cretaceous/Tertiary event. *Geology* **14**, 485–487.

581 Larsson L., Olsson G., Holst O. and Karlsson H.T. (1990) Pyrite oxidation by thermophilic
582 archaebacteria. *Appl. Environ. Microb*. **56**, 697–701.

583 Leclerc A. (1980) Room Temperature Mössbauer Analysis of Jarosite–Type Compounds.
584 *Phys. Chem. Minerals*. **6**, 327–334.

585 Lennie A. R. and Vaughan D. J. (1992) Kinetics of the marcasite–pyrite transformation:
586 An infrared spectroscopic study. *Am. Mineral*. **77**, 1166–117I.

587 Longworth G., Townsend M. G. and Ross C. A. M. (1986) Mössbauer spectra of several
588 sheet silicates in external magnetic field. *Hyperfine Interact*. **28**, 451–454.

589 Madsen D. E., Cervera-Gontard L., Kasama T., Dunin-Borkowski R. E., Koch C. B.
590 Hansen M. F. and Frandsen C., Morup, S. (2009) Magnetic fluctuations in nanosized
591 goethite (α-FeOOH). *J of Physics- Condensed Matter* **21**, 016007

592 Moshkovitz S. and Habib D. (1993) Calcareous nannofossil and dinoflagellate stratigraphy
593 of the Cretaceous–Tertiary boundary, Alabama and Georgia. *Micropaleontology* **39**,
594 167–191.

595 Mørup S., Madsen M. B., Franck J., Villadsen J. and Koch C. J. W. (1983) A new
596 interpretation of Mössbauer -spectra of microcrystalline goethite - super-
597 ferromagnetism or super-spin-glass behavior *J. Magn. Magn. Mater.* **40**, 163–174.

598 Nichols D. J. and Johnson K. R. (2002) Palynology and microstratigraphy of Cretaceous–
599 Tertiary boundary sections in southwestern North Dakota. In *The Hell Creek Formation*
600 *and the Cretaceous–Tertiary boundary in the northern Great Plains: An Integrated*
601 *continental record of the end of the Cretaceous* (eds. J. H. Hartman K. R. Johnson and
602 D. J. Nichols) Boulder, Colorado. *Geol. Soc. Spec. Paper,* vol. 361, 95–143.

603 Ocampo A., Vajda V. and Buffetaut E. (2006) Unravelling the Cretaceous–Paleogene (KT)
604 catastrophe: Evidence from flora fauna and geology. In *Biological Processes Associated with*
605 *Impact Events* (eds. C. Cockell, C. Koeberl and I. Gilmour) Springer –Verlag series, pp. 203–
606 227.

607 O'Keefe J. A. and Ahrens T. J. (1989) Impact production of CO_2 by the
608 Cretaceous/Tertiary extinction bolide and the resultant heating of the Earth. *Nature*
609 **338**, 247–249.

610 Peucker–Ehrenbrink B. and Jahn B–M. (2001) Rhenium–osmium isotope systematics and
611 platinum group element concentrations: Loess and the upper continental crust.
612 *Geochem. Geophys. Geosyst*. **2**, 2200, doi:10.1029/2001 GC000172.

613 Peucker–Ehrenbrink B., Bach W., Hart S. R., Blusztajn J. S. and Abbruzzese T. (2003)
614 Rhenium–osmium isotope systematics and platinum group element concentrations in
615 oceanic crust from DSDP/ODP Sites 504 and 417/418. *Geochem. Geophys. Geosyst.,*
616 **4**, 8911, doi: 10.1029/2002GC000414.

617 Peucker–Ehrenbrink B., Ravizza G. and Hofmann A. W. (1995) The marine $^{187}Os/^{186}Os$
618 record of the past 80 million years. *Earth Planet. Sci. Lett.* **130**, 155–167.

619 Pole M. and Vajda V. (2009) A new terrestrial Cretaceous-Paleogene site in New Zealand -
620 turnover in macroflora confirmed by palynology. *Cret. Res.* **30**, 917–938.

621 Pope K. O., Baines K. H., Ocampo A. C. and Ivanov B.A. (1994) Impact winter and the
622 Cretaceous/Tertiary extinctions: results of a Chicxulub asteroid impact model. *Earth*
623 *Planet Sci. Lett.* **128**, 718–725.

624 Raine J. I. (1984) Outline of a palynological zonation of the Cretaceous to Paleogene
625 terrestrial sediments in West Coast Region, South Island, New Zealand. *Report. New*
626 *Zeal. Geol. Surv. Rec* **109**, 82 pp.

627 Rancourt D. G. (1994) Inadequacy of Lorentzian–line doublets in fitting spectra arising
628 from quadrupole splitting distributions. *Phys. Chem. Mineral* **21**, 244–249.

629 Ravizza G. and Pyle D. (1997) PGE and Os isotoic analyses of single sample aliquots with
630 NiS fire assay preconcentration. *Chem. Geol* **141**, 251–268.

631 Robin E., Bonte P. H., Froget L., Jehanno C. and Rochia R. (1992) Formation of spinels in
632 cosmic objects during atmospheric entry: a clue to the Cretaceous–Tertiary event.
633 *Earth Planet. Sci. Lett*. **108**, 181–190.

634 Rohwerder T., Gehrke T., Kinzler K. and Sand W. (2003) Bioleaching review part A:
635 Progress in bioleaching: fundamentals and mechanisms of bacterial metal sulfide
636 oxidation. *Appl. Microbiol. Biot.* **63**, 239–248.

637 Rongchuan L., Shixin W., Yuanfu H., Weimin D. and Lirong C. (1986) A Mössbauer
638 investigation of the formation process of glauconite. *Hyperfine Interact.* **29**, 1085–
639 1088.

640 Schulte P., Deutsch A., Salge T., Berndt J., Kontny A., MacLeod K. G., Neuser R. D. and
641 Krumma S. (2009) A dual-layer Chicxulub ejecta sequence with shocked carbonates
642 from the Cretaceous–Paleogene (K–Pg) boundary, Demerara Rise, western Atlantic.
643 *Geochim. Cosmochim. Acta.* **73**, 1180–1204.

644 Schulte P., Alegret L., Arenillas I., Arz J. A., Barton P. J., Bown P. R., Bralower T.,
645 Christeson G., Claeys P., Cockell C., Collins G., Deutsch A., Goldin T., Goto K.,
646 Grajales-Nishimura J. M., Grieve R., Gulick S., Johnson K. R., Kiessling W., Koeberl
647 C., Kring D. A., MacLeod K. G., Matsui T., Melosh J., Montanari A., Morgan J., Neal
648 C., Norris R. D., Pierazzo E., Ravizza, G., Rebolledo-Vieyra M., Reimold W-U., Robin
649 E., Salge T., Speijer R. P., Sweet A. R., Urrutia-Fucugauchi J., Vajda V., Whalen M.
650 T., Willumsen P. S. (2010) The Chicxulub Impact and the Mass Extinction at the
651 Cretaceous-Paleogene Boundary. *Science* **327**, 1214–1218.

652 Sigurdsson H., Bonte P., Turpin L., Chaussidon M., Metrich N., Steinberg M., Pradel P. and
653 D'Hondt S. (1991a) Geochemical constraints on source region of Cretaceous/Tertiary
654 impact glasses. *Nature* **353**, 839–842.

655 Sigurdsson H., D'Hondt S., Arthur M., Bralower T. J., Zachos J. C., Van Fossen M. C. and
656 Channell J. E. T. (1991b) Glass from the Cretaceous/Tertiary boundary in Haiti.
657 *Nature* **349**, 482–487.

658 Smit J. and Kyte F. T. (1984) Siderophile–rich magnetic spheroids from the Cretaceous–
659 Tertiary boundary in Umbria, Italy. *Nature* **310**, 403–405.

660 Smit J. (1999) The global stratigraphy of the Cretaceous-Tertiary boundary impact ejecta:
661 *Ann. Rev. Earth Plan.* Sc **27**, 75–113.

662 Stephens J. R. and Kothari B. K. (1978) Laboratory analogues to cosmic dust. *Earth Moon*
663 *Planets* **19**, 139–152.

664 Stover L. E., Brinkhuis H., Damassa S. P., de Verteuil L., Helby R.J., Monteil E., Partridge A.
665 D., Powell A. J., Riding J. B., Smelror M. and Williams G. L. (1996) Mesozoic–
666 Tertiary dinoflagellates, acritarchs and prasinophytes. In *Palynology: principles and*
667 *applications* 1 (eds. J. Jansonius and D. C. Mcgregor), 641–750.

668 Vajda V. (1999). Miospores from Upper Cretaceous-Paleocene strata in northwestern Bolivia.
669 *Palynology* **23**, 183–198.

670 Vajda V. and McLoughlin S. (2005). A new Maastrichtian-Paleocene *Azolla* species from
671 Bolivia, with a comparison of the global record of coeval *Azolla* microfossils.
672 *Alcheringa* **29**, 305–329.

673 Vajda V., Raine J. I. and Hollis C. J. (2001) Indication of global deforestation at the
674 Cretaceous–Tertiary boundary by New Zealand fern spike. *Science* **294**, 1700–1702.

675 Vajda V. and Raine J. I. (2003) Pollen and spores in marine Cretaceous/Tertiary boundary
676 sediments at mid–Waipara River, North Canterbury, New Zealand. *New Zealand*
677 *Journal of Geology and Geophysics* **46**, 255–273.

678 Vajda V., Raine J. I., Hollis C. and Strong C. P. (2003) Global effects of the Chicxulub
679 asteroid impact on terrestrial vegetation– the palynological record from New Zealand
680 K–T boundary. In *Impact studies* (ed. P. Clayes) Springer –Verlag series, 57–74.

681 Vajda V. and McLoughlin S. (2004) Fungal Proliferation at the Cretaceous–Tertiary
682 Boundary. *Science* **303**, 1489.

683 Vajda V. and McLoughlin S. (2007) Extinction and recovery patterns of the vegetation across
684 Cretaceous–Palaeogene boundary – a tool for unravelling the causes of the end–Permian
685 mass–extinction. *Rev. Palaeobot. Palyno*. **144**, 99–112.

686 Vajda V., Raine, J. I. (2010) A palynological investigation of plesiosaur-bearing rocks from
687 the Upper Cretaceous Tahora Formation, Mangahouanga, New Zealand. *Alcheringa: An*
688 *Australasian Journal of Palaeontology* **131**, 1–16.

689 Verma H. C., Upadhyay C., Tripathi R. O., Tripathi A., Shukla A. D. and Bhandari N.
690 (2001) Nano–sized iron phases at the K/T boundaries revealed by Mössbauer
691 spectroscopy. *Lunar and Planet. Sci.* **XXXVII**, 1270–1271.

692 Villasante–Marcos V., Hollis C. J., Dickens G.R. and Nicolo M. J. (2009) Rock magnetic
693 properties across the Paleocene-Eocene Thermal Maximum in Marlborough, New
694 Zealand. *Geologica Acta* 7, 229–242.

695 Wagner U., Murad E., Knorr W. and Wagner F. E. (1990) Mössbauer study of illite clays
696 containing iron–rich impurities. *Hyperfine Interact*. **57**, 2313–2318.

697 Warren G., Speden I. G. (1978) The Piripauan and Haumurian stratotypes (Mata Series,
698 Upper Cretaceous) and correlative sequences in the Haumuri Bluff district of south
699 Marlborough. *New Zeal. Geol. Surv. Bull.* 92**,** 60pp.

700 Wdowiak T. J., Armendarez L. R., Agresti D. G., Wade M. L., Wdowial S. Y., Clayes P.
701 and Izett, G. (2001) Presence of an iron–rich nanophase material in the upper layer of
702 the Cretaceous–Tertiary boundary clay. *Meteorit. Planet. Sci*. **36**, 123–133.

703 Wigforss–Lange J., Vajda V. and Ocampo A. (2007) Rare earth elements (REE) and other trace
704 element concentrations in proximal Chicxulub ejecta deposits from northern Belize – support
705 for a single–impact scenario. *Meteorit. Planet. Sci*. **42**, 1871–1882.
706 Williams G. L., Brinkhuis H., Pearce M. A., Fensome R. A. and Weegink J. W. (2004)
707 Southern Ocean and global dinoflagellate cyst events compared: index events for the
708 Late Cretaceous–Neogene. In *Proceed. Ocean Drill. Prog., Sci. Res.* (eds. N. F. Exon, J.
709 P. Kenneth and M. J. Malone) 189, 1–98.
710 Willumsen P. S. (2000) Late Cretaceous to early Paleocene palynological changes in mid-
711 latitude Southern Hemisphere, New Zealand. In *Early Paleogene warm climates and*
712 *biosphere dynamic* (eds. B. Schmitz, B. Sundquist and F. P. Andreasson) ***GFF*** 122,
713 180–181.
714 Willumsen P. S. (2003) Marine palynology across the Cretaceous–Tertiary boundary in New
715 Zealand. Unpublished PhD Thesis, Victoria University of Wellington, Wellington, New
716 Zealand, 387 pp.
717 Willumsen P. S., (2004) Two new species of the dinoflagellate cyst genus *Carpatella*
718 Grigorovich 1969 from the Cretaceous–Tertiary transition in New Zealand. *Journal of*
719 *Micropalaeontology* **23**, 119–125.
720 Willumsen P. S. (2006) *Palynodinium minus* sp. nov., a new dinoflagellate cyst from the
721 Cretaceous–Paleogene transition in New Zealand; Its significance and palaeoecology.
722 *Cret. Res*. **27**, 954–963.
723 Willumsen P. S. (2010) Maastrichtian to Paleocene dinocysts from the Clarence Valley, South
724 Island, New Zealand. *Alcheringa* **35**, 1–42. ISSN 0311-5518.
725 Wilson G. J. (1984) New Zealand Late Jurassic to Eocene dinoflagellate biostratigraphy – a
726 summary. *Newsletters on stratigraphy* **13**, 104–117.

727 Wilson G. J. (1987) Dinoflagellate biostratigraphy of the Cretaceous–Tertiary boundary, mid–
728 Waipara River Section, North Canterbury, New Zealand. *New Zeal. Geol. Surv. Rec*. **20**,
729 8–16.
730 Zhou L., Kyte F. T. and Bohor B. F. (2001) Cretaceous/Tertiary boundary of DSDP Site
731 596, South Pacific. *Geology* **19**, 694–697.

732

733 **Figure Captions:**

734

735 **Fig. 1a.** Location of the Cretaceous-Paleogene (K-Pg) exposures of mid-Waipara River and
736 Compressor Creek, New Zealand.

737

738 **Fig. 1b.** Paleogeographical map of New Zealand showing the position of the investigated
739 localities 65 million years ago. Investigated sections marked with red.

740

741 **Fig. 2.** The sampled section at Compressor Creek, Greymouth coalfield, New Zealand (Scale;
742 measuring stick = 100 cm long).

743

744 **Fig. 3.** Powder X-ray diffraction results from the K-Pg boundary succession a) mid-Waipara
745 sample MW-13, containing glauconite, quartz, feldspar and gypsum. b) Compressor
746 Creek, sample CC-4, containing illite, quartz, kaolinite and pyrite.
747 C: chlorite; F: feldspar; I: illite; K: kaolinite; Q: quartz; S: smectite.
748

749

750 **Fig. 4.** Representative Mössbauer spectra of samples MW-10, 13 and 15 from the mid-
751 Waipara section, measured at 296K and 30K, respectively. Note the presence of the
752 sextet in MW-13 reflecting the presence of jarosite at the K-Pg boundary.

753

754 **Fig. 5.** Composite figure of results for the mid-Waipara sample set with lithological log and
755 microfossil zonations to the left.
756 **a)** Distribution of total $^{[6]}Fe^{3+}$ and $^{[6]}Fe^{2+}$ in glauconite at 296K.
757 **b**) Distribution of $^{[6]}Fe^{3+}$ in M1 and M2 in glauconite at 296K.

758 **c)** Distribution of Fe species for measurements at 30K. Note the anomaly of Fe^{3+} due to
759 the presence of jarosite at samples MW-12 and MW-13.
760
761 **Fig. 6.** Representative Mössbauer spectra from the Compressor Creek section, measured at
762 296K and 20K respectively. Note the line broadening for the samples at and below the
763 K-Pg for the 296K analyses and the corresponding sextets for the 20K analyses.
764
765 **Fig. 7.** Composite figure of Mössbauer results from the Compressor Creek sample set with
766 lithological log and pollen zonations to the left. SIRMis the saturation isothermal
767 remanent magnetization and Hcr is the remanence coercivity
768
769 **Fig. 8a**. Palynological results from mid-Waipara.
770 Pollen and spore abundances and distribution of key-species. The miospores have been
771 grouped within their affinity: 1. Ferns, 2. Conifers, 3. Angiosperms (flowering plants).
772 Note the significant increase in fern spores coincident with the boundary, sample 13.
773 Dinoflagellates; distribution of key-species. Note the appearance of Paleogene index
774 species in sample 13.
775
776 **Fig. 8b**. Palynological results from Compressor Creek.
777 Pollen and spore abundances and distribution of key-species. The pollen and spores
778 have been grouped within their affinity: 1. Ferns, 2. Conifers, 3. Angiosperms. Note the
779 significant increase in fern spores coincident with the K-Pg boundary.
780
781 **Table 1**. Relative distribution (in %) of $^{[6]}Fe^{2+}$ and $^{[6]}Fe^{3+}$ in glauconite for the Mid-Waipara
782 samples from Mössbauer spectroscopy measured at 296K (Fig. 5a), distribution of $^{[6]}Fe^{3+}$

783 for the octahedrally coordinated M1 and M2 sites in glauconite measured at 296K (Fig.
784 5b), and distribution of $^{[6]}Fe^{2+}$ and $^{[6]}Fe^{3+}$ of glauconite and $^{[6]}Fe^{3+}$ of jarosite taken at
785 30K (Fig. 5c). M1 and M2 are two non equivalent octahedral sites where the ferrous and
786 ferric iron is accommodated. T is the sum of ferrous and ferric iron in M1 and M2,
787 respectively.
788
789 **Table 2**. The relative distribution in % - obtained by Mössbauer spectroscopy - of ferrous
790 (Fe^{2+}), and paramagnetic ferric (Fe^{3+}PM) in chlorite and illite; and the distribution of
791 super-paramagnetic ferric iron (Fe^{3+}SPM) in goethite for the samples from Compressor
792 Creek.
793
794 **Table 3**. Osmium isotope composition and platinum group element concentrations.
795 **Notes**: * - Cretaceous-Paleogene boundary. n.d. - not determined. r – replicate. [1] -
796 concentrations are corrected for instrumental background and typical analytical blank
797 concentrations of 0.6 pg Os/g, 1.3 pg Ir/g, 14 pg Pt/g and 26 pg Pd/g (see Peucker-
798 Ehrenbrink et al., 2003, for details). Osmium concentrations are determined using three
799 isotope ratios, Pt and Pd are calculated using two isotope ratios, while Ir concentrations are
800 based on the 191/193 mass ratio. Concentrations determined by different isotope ratios
801 typically agree to better than 2%.

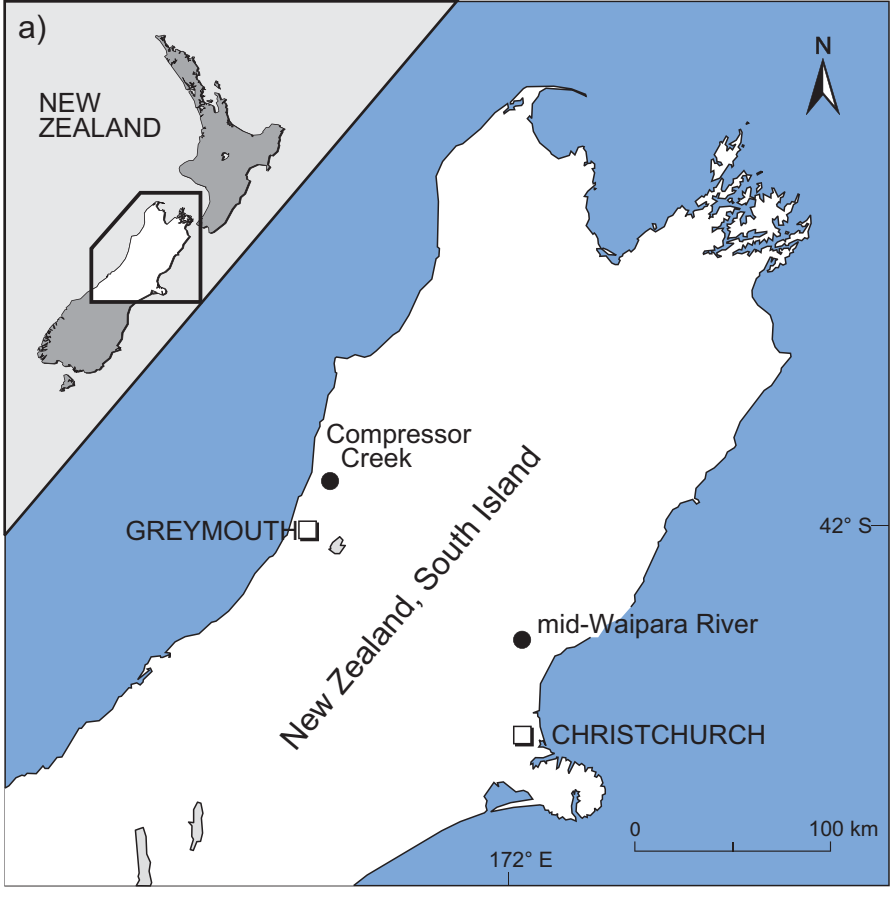
a)
NEW ZEALAND
N
Compressor Creek
GREYMOUTH
New Zealand, South Island
42° S
mid-Waipara River
CHRISTCHURCH
0
100 km
172° E

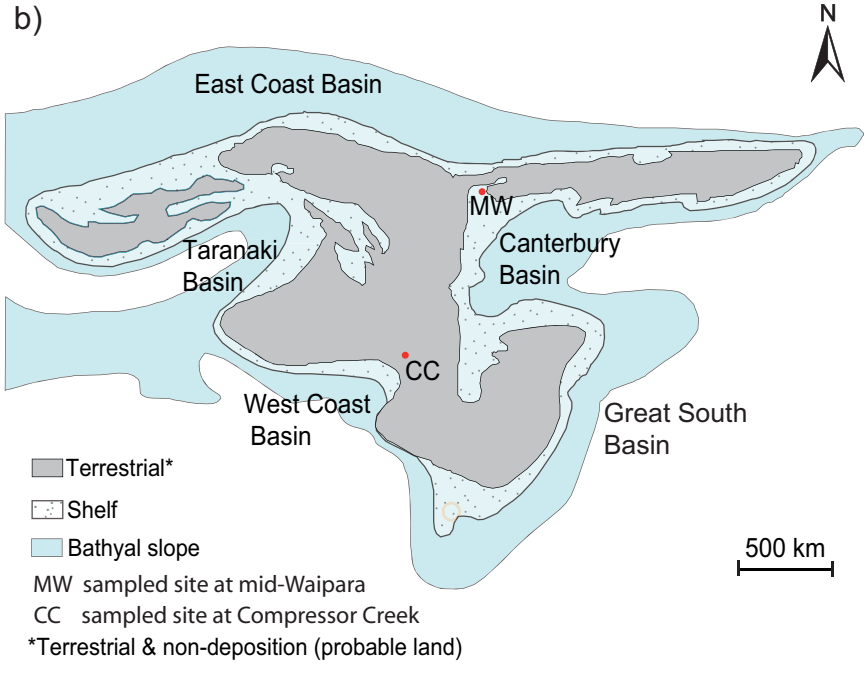
b)
N
East Coast Basin
MW
Taranaki Basin
Canterbury Basin
CC
West Coast Basin
Great South Basin
Terrestrial*
Shelf
Bathyal slope
500 km
MW sampled site at mid-Waipara
CC sampled site at Compressor Creek
*Terrestrial & non-deposition (probable land)

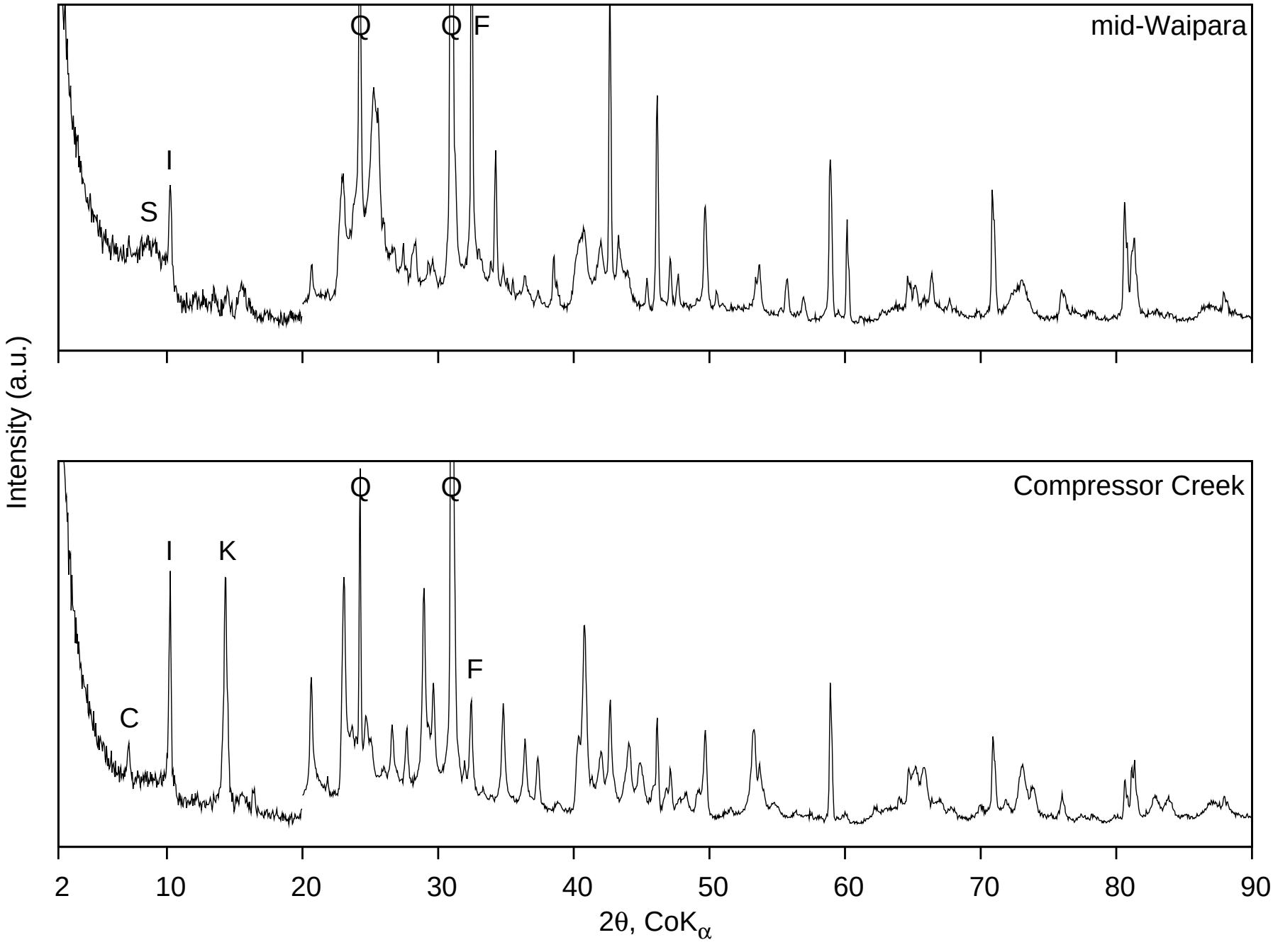
mid-Waipara
Q
Q
F
I
S
Compressor Creek
Q
Q
I
K
F
C
Intensity (a.u.)
2
10
20
30
40
50
60
70
80
90
2θ, CoKα

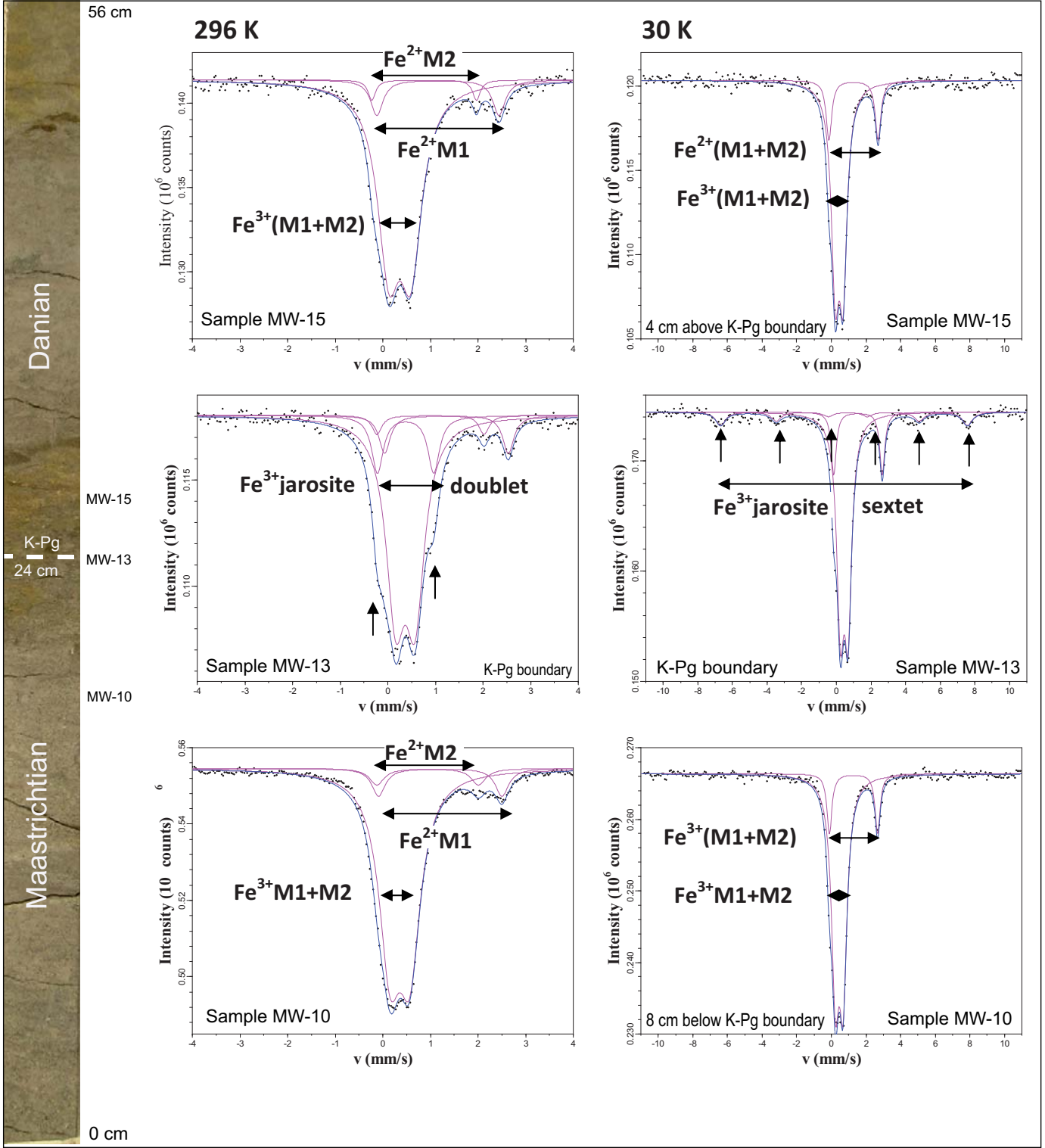
56 cm
296 K
30 K
Danian
Maastrichtian
K-Pg
24 cm
MW-15
MW-13
MW-10
0 cm
Fe2+M2
Fe2+M1
Fe3+(M1+M2)
Sample MW-15
Fe2+(M1+M2)
Fe3+(M1+M2)
4 cm above K-Pg boundary
Sample MW-15
Fe3+jarosite
doublet
Sample MW-13
K-Pg boundary
Fe3+jarosite
sextet
K-Pg boundary
Sample MW-13
Fe2+M2
Fe2+M1
Fe3+M1+M2
Sample MW-10
Fe3+(M1+M2)
Fe3+M1+M2
8 cm below K-Pg boundary
Sample MW-10
Intensity (10^6 counts)
v (mm/s)

Period
Age
Pollen zone
Dinoflagellate zone
cm
Lithology
Sample numbers
CRETACEOUS
PALEOGENE
Maastrichtian
Danian
PM2
PM3
Manumiella druggii Interval Zone
Trithyrodinium evittii Interval Zone
K-Pg
a)
b)
c)
Fe2+
Fe3+
Fe3+ M1
Fe3+ M2
Fe2+
Fe3+
Fe3+ in jarosite
0 20 40 80 100%
10 30 70 90 %
10 20%
70 90 0 20%

296 K

20 K

CC-5

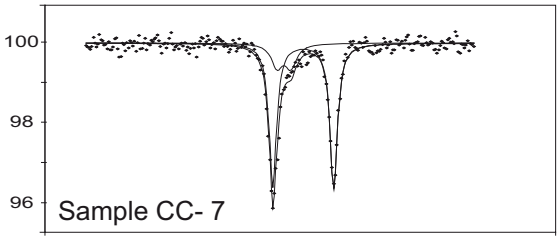

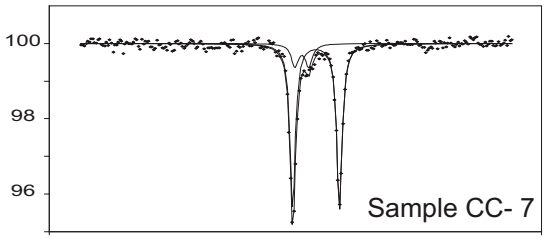

CC-4

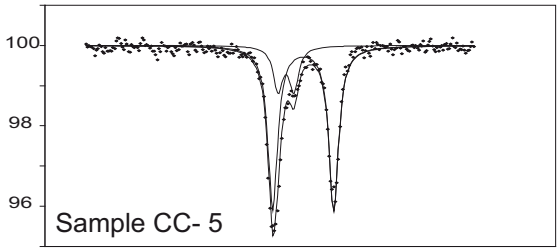

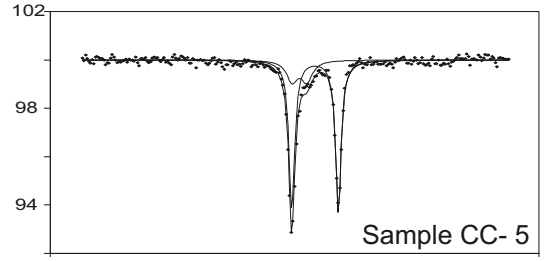

CC-3

CC-2

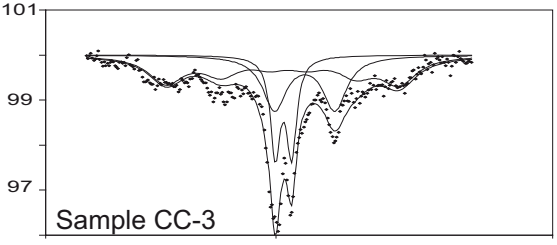

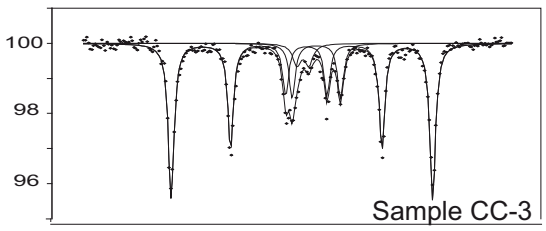

CC-1

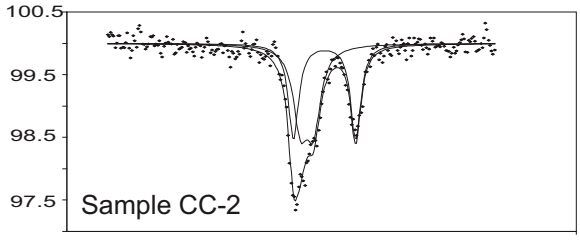

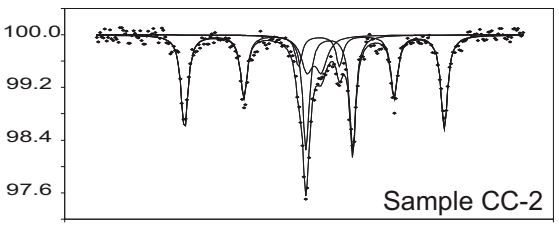

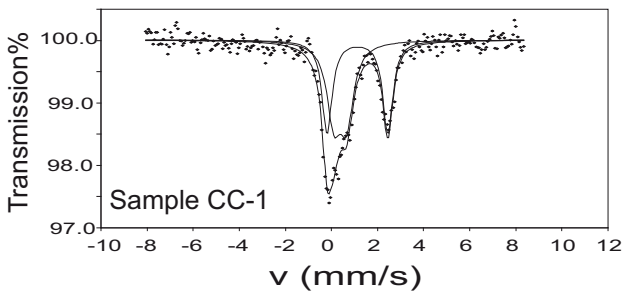

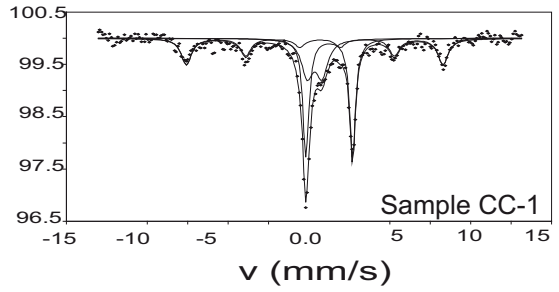

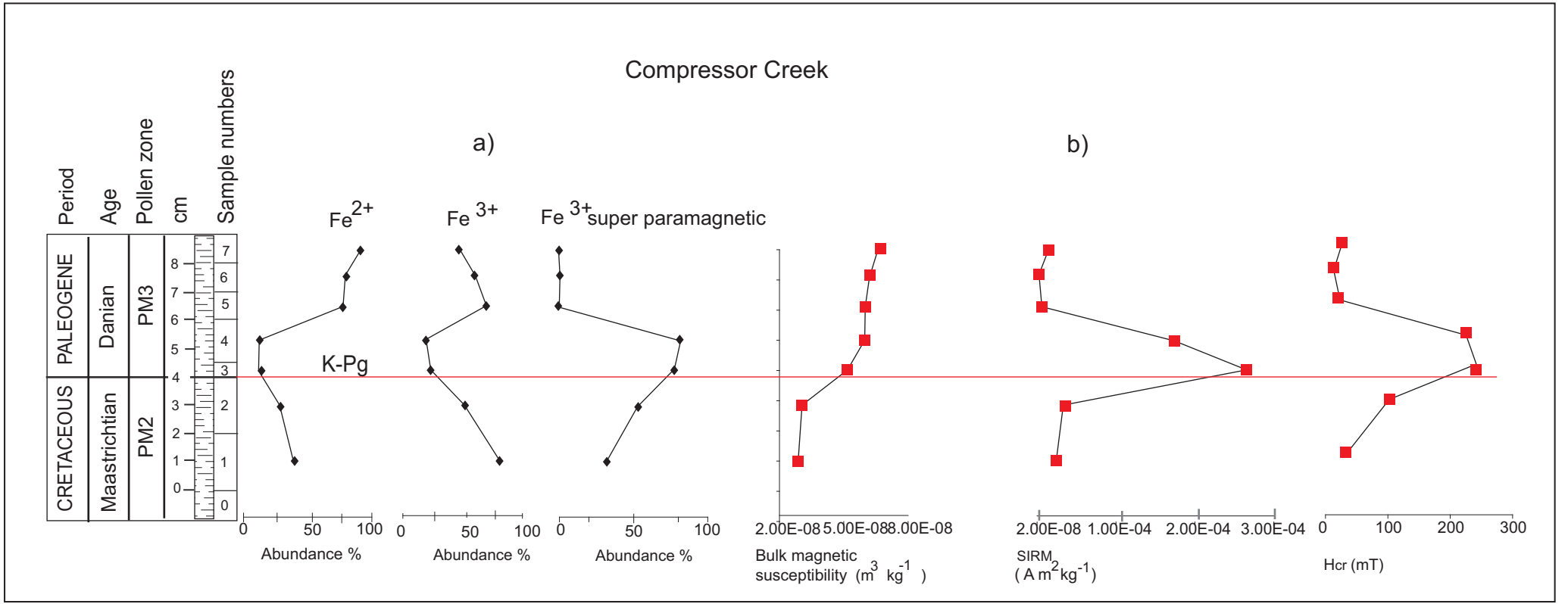
Compressor Creek
Period
Age
Pollen zone
cm
Sample numbers
PALEOGENE
CRETACEOUS
Danian
Maastrichtian
PM3
PM2
K-Pg
a)
b)
Fe2+
Fe 3+
Fe 3+super paramagnetic
Abundance %
Bulk magnetic susceptibility (m3 kg-1)
SIRM (A m2kg-1)
Hcr (mT)

meter
Ground ferns
35
30
25
20
15
10
5
0
20
100 %
Close up of
fern-spike interval
Age
Pollen zone
Dinoflagellate zone
cm
Lithology
Sample number
PALEOGENE
Danian
PM3
Trithyrodinium evittii
Interval Zone
CRETACEOUS
Maastrichtian
PM2
Manumiella druggii
Interval Zone
40
30
20
10
0
26
24
22
16/17
14/15
12/13
11
10
8
6
4
1
cm
Ferns
Conifers
Flowering plants
45
40
35
30
25
20
15
10
5
0
20 40 60 80 100 20 40 60 20 %
Dinoflagellate key species
first Danian appearance
S. inornata
C. cornuta
D. californicum
T. evittii
M. tenella

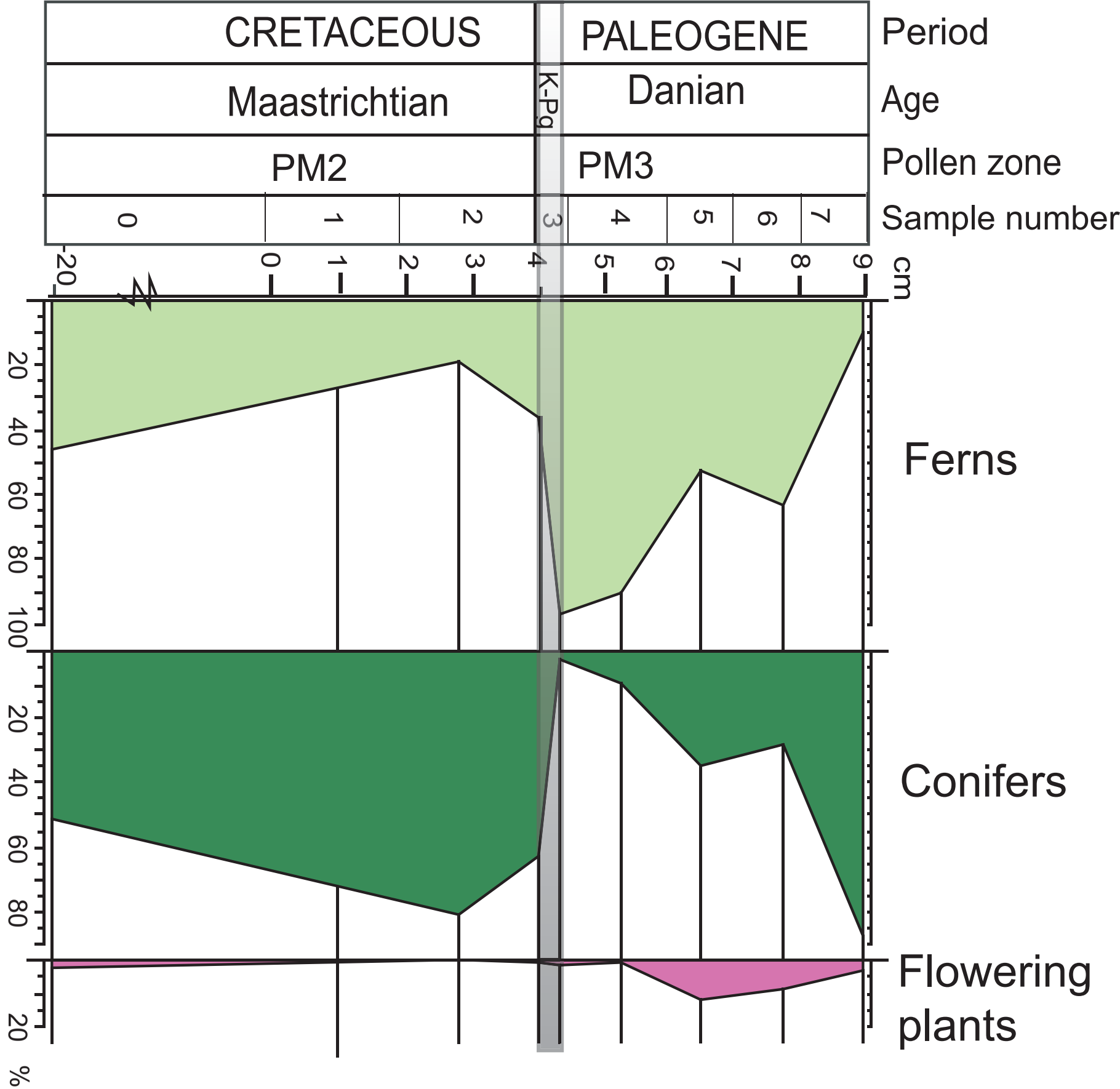
CRETACEOUS
PALEOGENE
Period
Maastrichtian
K-Pg
Danian
Age
PM2
PM3
Pollen zone
0
1
2
3
4
5
6
7
Sample number
-20
0
1
2
3
4
5
6
7
8
9
cm
20
40
60
80
100
Ferns
20
40
60
80
Conifers
Flowering plants
20
%

mid-Waipara sample no.	cm from base of section	Fe^{2+}(T)	Fe^{3+}(T)	Fe^{2+}M1	Fe^{3+}M1	Fe^{2+}M2	Fe^{3+}M2
28	54-56	15.1	84.9	32.0	16.0	68.0	84.0
27	52-54	18.5	81.5	32.0	16.0	68.0	84.0
26	50-52	21.7	78.3	24.3	8.8	75.7	91.2
25	48-50	25.6	74.4	26.0	14.4	74.0	85.6
24	46-48	20.3	79.7	27.9	12.9	72.1	87.1
23	44-46	21.9	78.1	28.0	10.4	71.7	89.6
22	42-44	21.2	78.8	28.0	12.2	72.0	87.8
21	40-42	20.4	79.6	32.6	6.5	67.4	93.5
20	38-40	15.5	84.5	33.1	22.9	66.9	77.1
19	36-38	17.7	82.3	22.3	14.6	77.7	85.4
18	34-36	18.4	81.6	32.0	13.0	68.0	87.0
17	32-34	16.0	84.0	38.0	25.2	61.8	74.8
16	30-32	21.9	78.1	28.1	13.2	71.9	86.8
15	28-30	18.7	81.3	32.1	21.2	67.9	78.8
14	26-28	19.3	80.7	37.4	11.6	62.6	88.4
13	24-26	15.9	84.1	29,0	31.2	71.0	68.8
12	22-24	17.8	82.2	26,0	27.4	74.0	72.6
11	20-22	19.4	80.6	40,0	11.5	60.2	88.5
10	18-20	16.8	83.2	34.8	13.5	65.2	86.5
9	16-18	17.3	82.7	29,0	13.0	71.3	87.3
8	14-16	21.7	78.3	27.2	9.2	72.8	90.8
7	12-14	19.8	80.2	37.8	8.9	62.2	91.1
6	10-12	21.9	78.1	24.9	10.3	75.1	89.7
5	8-10	20.1	79.9	27.2	9.2	72.8	90.8
4	6-8	19.7	80.3	30.4	8.3	69.6	91.7
3	4-6	19.2	80.8	27.4	12.1	72.6	87.9
2	2-4	19.9	80.1	28.9	11.2	71.1	88.8
1	0-2	21.5	78.5	35.5	24.0	64.5	76.0

Compressor C. sample no.	cm from base of section	Fe^{3+}(PM)	Fe^{2+}	Fe^{3+}(SPM)
7	8-9	14.8	85.2	0
6	7-8	18	82.0	0
5	6-7	21.1	78.9	0
4	4.5-6	6	13.3	80.7
3	4-4.5	7.2	14.6	78.2
2	2-4	15.8	30.7	53.5
1	0-2	24.7	43.1	32.2

Compressor C. sample no.	cm from base of section	$^{187}Os/^{188}Os$	±2σ	Os[1] pg/g	Ir[1] pg/g	Pt[1] pg/g	Pd[1] pg/g
7	8-9	0.3487	0.0021	50	102	172	739
4	4.5-6	0.2529	0.0015	119	161	559	1808
4r	4.5-6	0.2577	0.0014	120	n.d.	n.d.	n.d.
3	4-4.5	0.2040	0.0005	172	176	568	1465
1	0-2	0.1993	0.0010	165	153	610	1169
mid-Waipara sample no.							
14	26-28	0.2670	0.0007	2162	233	498	770
13*	24-26	0.2692	0.0012	1200	321	677	780
12	22-24	0.3136	0.0010	1022	304	613	813
11	20-22	0.3391	0.0010	834	273	534	768